High-order bound-preserving discontinuous Galerkin methods for compressible miscible displacements in porous media on triangular meshes[1]

Nattaporn Chuenjarern[2] Ziyao Xu[3] and Yang Yang[4]

Abstract

In this paper, we develop high-order bound-preserving (BP) discontinuous Galerkin (DG) methods for the coupled system of compressible miscible displacements on triangular meshes. We consider the problem with multi-component fluid mixture and the (volumetric) concentration of the jth component, c_j, should be between 0 and 1. There are three main difficulties. Firstly, c_j does not satisfy a maximum-principle. Therefore, the numerical techniques introduced in (X. Zhang and C.-W. Shu, Journal of Computational Physics, 229 (2010), 3091-3120) cannot be applied directly. The main idea is to apply the positivity-preserving techniques to all $c_j's$ and enforce $\sum_j c_j = 1$ simultaneously to obtain physically relevant approximations. By doing so, we have to treat the time derivative of the pressure dp/dt as a source in the concentration equation and choose suitable fluxes in the pressure and concentration equations. Secondly, it is not easy to construct first-order numerical fluxes for interior penalty DG methods on triangular meshes. One of the key points in the high-order BP technique applied in this paper is the combination of high-order and lower-order numerical fluxes. We will construct second-order BP schemes and use the second-order numerical fluxes as the lower-order one. Finally, the classical slope limiter cannot be applied to c_j. To construct the BP technique, we will not approximate c_j directly. Therefore, a new limiter will be introduced. Numerical experiments will be given to demonstrate the high-order accuracy and good performance of the numerical technique.

Key Words: compressible miscible displacements, bound-preserving, high-order, discontinuous Galerkin method, triangular meshes, multi-component fluid, flux limiter

1 Introduction

In this paper, we are interested in constructing high-order bound-preserving discontinuous Galerkin (DG) schemes for compressible miscible displacements in porous media on triangular meshes. We consider the fluid mixture with N components and the governing equations over the computational domain $\Omega = [0,1] \times [0,1]$ read

$$d(\mathbf{c})\frac{\partial p}{\partial t} + \nabla \cdot \mathbf{u} = d(\mathbf{c})\frac{\partial p}{\partial t} - \nabla \cdot \left(\frac{\kappa(x,y)}{\mu(\mathbf{c})}\nabla p\right) = q, \ \ (x,y) \in \Omega, \ \ 0 < t \leq T, \tag{1.1}$$

[1]Research supported by the NSF grant DMS-1818467

[2]Department of Mathematical Sciences, Michigan Technological University, Houghton, MI 49931. E-mail: nchuenja@mtu.edu

[3]Department of Mathematical Sciences, Michigan Technological University, Houghton, MI 49931. E-mail: ziyaox@mtu.edu

[4]Department of Mathematical Sciences, Michigan Technological University, Houghton, MI 49931. E-mail: yyang7@mtu.edu

$$\phi\frac{\partial c_j}{\partial t}+\nabla(\mathbf{u}\cdot c_j)-\nabla\cdot(\mathbf{D}\nabla c_j)=\tilde{c}_j q-\phi c_j z_j p_t,\ \ (x,y)\in\Omega,\ \ 0<t\le T,\ j=1,\cdots,N-1, \quad (1.2)$$

where the dependent variables are the pressure in fluid mixture denoted by p, the Darcy velocity of the mixture (volume flowing across a unit across-section per unit time) denoted by $\mathbf{u}$ and the concentration of interested species measured in amount of species per unit volume denoted by $\mathbf{c}=(c_1,\cdots,c_N)^T$, with c_j being the concentration of the jth component. ϕ and κ are the porosity and permeability of the rock, respectively. μ refer to the concentration-dependent viscosity. q is the external volumetric flow rate, and $\tilde{c}_j$ is the concentration of the fluid in the external flow. $\tilde{c}_j$ must be specified at points where injection ($q>0$) takes place, and is assumed to be equal to c_j at production points ($q<0$). The diffusion coefficient $\mathbf{D}$ is symmetric and arises from two aspects: molecular diffusion, which is rather small for field-scale problems, and dispersion, which is velocity-dependent, in the petroleum engineering literature. Its form is

$$\mathbf{D}=\phi(x,y)(d_{\text{mol}}\mathbf{I}+d_{\text{long}}|\mathbf{u}|\mathbf{E}+d_{\text{tran}}|\mathbf{u}|\mathbf{E}^{\perp}), \quad (1.3)$$

where $\mathbf{E}$, a 2×2 matrix, represents the orthogonal projection along the velocity vector given as

$$\mathbf{E}=(e_{ij}(\mathbf{u}))=\left(\frac{u_i u_j}{|\mathbf{u}^2|}\right),\ \ \mathbf{u}=(u_1,u_2),$$

and $\mathbf{E}^{\perp}=\mathbf{I}-\mathbf{E}$ is the orthogonal complement. The diffusion coefficient d_{long} measures the dispersion in the direction of the flow and d_{tran} shows that transverse to the flow. To ensure the stability of the scheme, $\mathbf{D}$ is assumed to be strictly positive definite in almost all of the previous works. In this paper, we assume $\mathbf{D}$ to be positive semidefinite. Moreover, the pressure is uniquely determined up to a constant, thus we assume $\int_\Omega p\ dxdy=0$ at $t=0$. However, this assumption is not essential. Other coefficients can be stated as follows:

$$c_N=1-\sum_{j=1}^{N-1}c_j,\quad d(\mathbf{c})=\phi\sum_{j=1}^{N}z_j c_j,$$

where z_j is the compressibility factor of the jth component of the fluid mixture. In this paper, we consider homogeneous Neumann boundary conditions

$$\mathbf{u}\cdot\mathbf{n}=0,\quad (\mathbf{D}\nabla c-c\mathbf{u})\cdot\mathbf{n}=0,$$

where $\mathbf{n}$ is the unit outer normal of the boundary $\partial\Omega$. Moreover, the initial solutions are given as

$$c_j(x,y,0)=c_{j_0}(x,y),\quad p(x,y,0)=p_0(x,y),\quad (x,y)\in\Omega.$$

The miscible displacements in porous media were first presented in [9, 10], where mixed finite element methods were applied. Later, the compressible problem was studied in [11] and the optimal order estimates in L^2-norm and almost optimal order estimates in L^∞-norm were given in [5]. Subsequently, many new numerical methods were introduced, such as the finite difference method [41, 42, 43], characteristic finite element method [21], splitting positive definite mixed element method [34] and H1-Galerkin mixed method [3]. Besides the above, in [29], an accurate and efficient simulator was developed for problems with wells. Later, the authors introduced an

Eulerian-Lagrangian localized adjoint method to solve the transport partial differential equation for concentration, while a mixed finite element method to solve the pressure equation [28]. Recently, DG methods have been popular to solve compressible miscible displacements in porous media [7, 8, 35, 36, 17, 37, 40]. Some special numerical techniques were introduced to control the jumps of numerical approximations as well as the nonlinearality of the convection term. Besides the above, there were also significant works discussing the DG methods for incompressible miscible displacements, see e.g. [1, 18, 20, 22, 25, 26, 30] and for general porous media flow, see e.g. [2, 13, 12, 27] and the references therein. However, no previous works above focused on the bound-preserving techniques. In many numerical simulations, the approximations of c_j can be placed out of the interval $[0, 1]$. Especially for problems with large gradients, the value of $d(\mathbf{c})$ might be negative, leading to ill-posedness of the problem, and the numerical approximations will blow up. We will use numerical experiments to demonstrate this point in Section 5. In [16], we have introduced second-order bound-preserving DG methods on rectangular meshes for two-component miscible displacements in porous media. In this paper, we will extend the idea to multi-component miscible displacements and construct high-order bound-preserving techniques on triangular meshes. Moreover, the idea can be extended to incompressible flows with some minor changes.

The DG method gained even greater popularity for good stability, high-order accuracy, and flexibility on h-p adaptivity and on complex geometry. In 2010, the genuinely maximum-principle-satisfying high-order DG and finite volume schemes were constructed in [44] by Zhang and Shu, the extension to unstructured meshes was given in [47]. After that, the idea was applied to many problems such as compressible Euler equations [45, 46], hyperbolic equations involving δ-singularities [38, 39, 49], relativistic hydrodynamics [23] and shallow water equations [31], etc. The basic idea is to take the test function to be 1 in each cell to obtain an equation of the numerical cell average of the target variable, say r, and prove the cell average, $\bar{r}$, is within the desired bounds. Then we can apply a slope limiter to the numerical approximation and construct a new one

$$\tilde{r} = \bar{r} + \theta(r - \bar{r}), \quad \theta \in [0, 1]. \tag{1.4}$$

If the problem has only one lower bound zero, the technique is also called positivity-preserving technique. Thanks to the limiter, the whole algorithm were proved to be L^1-stable [39, 23] for some complicated systems. Moreover, the technique does not rely on the trouble cell detector and the limiter keeps the high-order accuracy in regions with smooth solutions for scalar equations [44]. In case of convection-diffusion equations, the same idea was applied to construct genuinely second-order maximum-principle-satisfying DG method on unstructured meshes [48]. Recently, the flux limiter [19, 32, 33] and third-order maximum-principle-preserving direct DG method [4] were also introduced. However, it is not easy to apply the flux limiter to unstructured meshes since the lower order fluxes are not easy to construct, and the only work available is [6] in which the technique for hyperbolic equations was analyzed, and no previous works aimed to discuss convection-diffusion equations. In this paper, we will extend the ideas in [32, 44] and construct high-order bound-preserving DG methods for multi-component compressible miscible displacements. However, there are significant differences from previous techniques. First of all, most of the problems in [32, 44] satisfy maximum-principles while the concentration c_j in (1.2) does not. To solve this problem, we would like to apply the positivity-preserving technique to each c_j and enforce $\sum_j c_j = 1$. Secondly, the high-order positivity-preserving technique in this paper is based on the flux limiter [19, 32].

The basic idea is to combine higher order and lower order fluxes to construct a new one which yield positive numerical cell averages. However, for triangular meshes, first-order fluxes are not easy to construct. Therefore, we will consider the second-order flux as the lower order one. Finally, to obtain the equation satisfied by the cell averages, we need to numerically approximate $r_j = \phi c_j$ instead of c_j. By doing so, the upper bound of r_j is not a constant and the limiter (1.4) may fail to work, since such a θ may not exist (see the counterexample in [16]). Moreover, the limiter applied in [16] is not straightforward extendable to multi-component problems, since we cannot simply set the upper bound of c_j to be 1 if the fluid mixture contains more than two components. Therefore, a new bound-preserving limiter will be introduced. In summary, the whole algorithm can be separated into three parts. We first treat p_t as another source in (1.2) to obtain the positivity of c_j by the flux limiter [19, 32]. Then we choose consistent fluxes (see Definition 2.1) with suitable parameter in the flux limiter in the concentration and pressure equations to obtain the positivity of $1-\sum_{j=1}^{N-1} c_j$. More precisely, in our analysis, instead of solving p and c_j, $j = 1, \cdots, N-1$, we rewrite (1.1) and (1.2) into a system of c_j, $j = 1, \cdots, N$ and enforce $\sum_{i=j}^{N} c_j = 1$ by choosing consistent fluxes. Finally, we will introduce a new limiter to obtain physically relevant numerical approximations.

The paper is organized as follows: we first discuss the DG scheme in two dimension on triangular mesh in Section 2. In Section 3, we demonstrate the bound-preserving technique for second-order scheme. The high-order bound-preserving technique with flux limiter will be given in Section 4. In Section 5, some numerical experiments and results will be shown. We will end in Section 6 with concluding remarks.

2 The DG scheme

In this section, we will construct the DG scheme for compressible miscible displacements in porous media. We first demonstrate the notations to be used throughout the paper. We consider triangular meshes and denote Ω_h to be the set of cells. For any $K \in \Omega_h$, we denote the three edges of K to be e_K^i $(i = 1, 2, 3)$, with corresponding lengths ℓ_K^i $(i = 1, 2, 3)$ and unit outer normal vectors $\boldsymbol{\nu}_i$ $(i = 1, 2, 3)$. We also denote the neighboring triangle along e_K^i as K_i. We use Γ for all the cell interfaces, and $\Gamma_0 = \Gamma \setminus \partial\Omega$ for all the interior ones. For any $e \in \Gamma$, denote $|e|$ to be the length of e. Let $u^{\pm}$ denote the numerical solution on the edges, evaluated from K or K_i. The $'\pm'$ for each edge e_K^i is determined by the inner product of $\boldsymbol{\nu}_i$ and a predetermined constant vector $\boldsymbol{\nu}_0$ which is not parallel to any edge in the mesh: for each edge e_K^i in the cell K,

$$\boldsymbol{u}^- = \boldsymbol{u}_K, \quad \boldsymbol{u}^+ = \boldsymbol{u}_{K_i}, \quad \text{if } \boldsymbol{\nu}_0 \cdot \boldsymbol{\nu}_i > 0,$$

$$\boldsymbol{u}^+ = \boldsymbol{u}_K, \quad \boldsymbol{u}^- = \boldsymbol{u}_{K_i}, \quad \text{if } \boldsymbol{\nu}_0 \cdot \boldsymbol{\nu}_i < 0.$$

Moreover, we define $\boldsymbol{n}_e$ as the unit outer normal of each edge $e \in \Gamma_0$ such that $\boldsymbol{n}_e \cdot \boldsymbol{\nu}_0 > 0$ and define the jump and average of any function v at the cell interface e as

$$[v]_e = v_e^+ - v_e^-, \quad \{v\}_e = \frac{1}{2}(v_e^+ + v_e^-).$$

We also denote $\partial\Omega_+ = \{e \in \partial\Omega : \mathbf{n} \cdot \boldsymbol{\nu}_0 > 0\}$, where $\mathbf{n}$ is the unit outer normal of $\partial\Omega$ and $\partial\Omega_- = \partial\Omega \backslash \partial\Omega_+$. The finite element space is chosen as

$$W_h = \{z : z|_K \in P^k(K),\ \forall K \in \Omega_h\},$$

where $P^k(K)$ denotes polynomials of degree at most $k \geq 1$ in K.

To construct the DG method, we first rewrite the system (1.1)-(1.2) into the following form

$$d(\mathbf{c})p_t + \nabla \cdot \mathbf{u} = q, \tag{2.1}$$

$$a(\mathbf{c})\mathbf{u} = -\nabla p, \tag{2.2}$$

$$(\phi c_j)_t + \nabla \cdot (\mathbf{u}c_j) - \nabla \cdot (\mathbf{D}(\mathbf{u})\nabla c_j) = \tilde{c}_j q - \phi c_j z_j p_t, \quad j = 1, 2, \cdots, N-1, \tag{2.3}$$

where $a(\mathbf{c}) = \dfrac{\mu(\mathbf{c})}{\kappa}$.

Next, we would like to demonstrate the key points in this paper that are quite different from most of the previous works.

1. Approximate $r_j = \phi c_j$ instead of c_j. We cannot simply take the test function to be 1 to obtain the cell average of c_j.

2. Treat p_t in (2.3) as a source to apply the positivity-preserving techniques.

3. Apply flux limiters to the high-order scheme by combining the second- and high-order fluxes.

4. Suitably choose the parameters in the flux limiter to obtain consistent fluxes for (2.1) and (2.3) to make $\bar{r_j} < \bar{\phi}$, where $\bar{r}_j$ and $\bar{\phi}$ are the cell averages of r_j and ϕ, respectively.

5. Take the L^2-projection of ϕ into W_h, denoted as Φ, and use which as the new approximation of the porosity.

6. Construct a new limiter to maintain the cell average $\bar{r}_j$ and modify the numerical approximations of r_j such that $0 < r_j < \Phi$, which further yields $c_j = P_k\left\{\dfrac{r_j}{\Phi}\right\} \in [0, 1]$, where P_k is the L^2-projection projection into W_h is $k \geq 2$ while $P_1 u|_K$ is the interpolation of u at the three vertices of cell K.

For simplicity, if not otherwise stated, we use $p, \mathbf{u}, c_j, r_j,\ j = 1, 2, \cdots, N$ as the numerical approximations from now on. Then the DG scheme for (2.1) - (2.3) is to find $p, r_j \in W_h$ and

$\mathbf{u} \in \mathbf{W}_h = W_h \times W_h$ such that for any $\xi, \zeta \in W_h$ and $\boldsymbol{\eta} \in \mathbf{W}_h$,

$$(\tilde{d}(\mathbf{r})p_t, \xi) = (\mathbf{u}, \nabla\xi) + \sum_{e\in\Gamma_0}\int_e \hat{\mathbf{u}}\cdot\boldsymbol{n}_e[\xi]ds + (q,\xi), \tag{2.4}$$

$$(a(\mathbf{c})\mathbf{u}, \boldsymbol{\eta}) = (p, \nabla\cdot\boldsymbol{\eta}) + \sum_{e\in\Gamma}\int_e \hat{p}[\boldsymbol{\eta}\cdot\boldsymbol{n}_e]ds, \tag{2.5}$$

$$\begin{aligned}(r_{j_t}, \zeta) = &(\boldsymbol{u}c_j - \boldsymbol{D}(\boldsymbol{u})\nabla c_i, \nabla\zeta) + (\check{c}_j q - r_j z_j p_t, \zeta) + \sum_{e\in\Gamma_0}\int_e \widehat{\boldsymbol{u}c_j}\cdot\boldsymbol{n}_e[\zeta]ds \\ &- \sum_{e\in\Gamma_0}\int_e\left(\{\boldsymbol{D}(\boldsymbol{u})\nabla c_j\cdot\boldsymbol{n}_e\}[\zeta] + \{\boldsymbol{D}(\boldsymbol{u})\nabla\zeta\cdot\boldsymbol{n}_e\}[c_j] + \frac{\tilde{\alpha}}{|e|}[c_j][\zeta]\right)ds,\end{aligned} \tag{2.6}$$

where

$$c_j = P_k\left\{\frac{r_j}{\Phi}\right\}, \quad \tilde{d}(\mathbf{r}) = \sum_{j=1}^{N} z_j r_j, \quad (u,v) = \int_K uvdx, \quad \check{c}_j = \begin{cases} \tilde{c}_j, & q > 0, \\ \frac{r_j}{\Phi}, & q < 0. \end{cases}$$

In (2.4)-(2.6), $\hat{p}, \hat{\boldsymbol{u}}$ and $\widehat{\boldsymbol{u}c_j}$ are the numerical fluxes. We use alternating fluxes for the diffusion term and for any $e \in \Gamma_0$

$$\hat{\boldsymbol{u}}|_e = \boldsymbol{u}^+|_e, \quad \hat{p}|_e = p^-|_e, \tag{2.7}$$

and on $\partial\Omega$ we take

$$\hat{p}|_e = p^-|_e, \ \forall e \in \partial\Omega^+, \quad \hat{p}|_e = p^+|_e, \ \forall e \in \partial\Omega^-.$$

For the convection term, for any $e \in \Gamma_0$ we take

$$\widehat{\boldsymbol{u}c_j} = \boldsymbol{u}^+ c_j^+ - \alpha[c_j]\mathbf{n}_e. \tag{2.8}$$

In (2.6) and (2.8), α and $\tilde{\alpha}$ are two positive constants to be chosen by the bound-preserving technique. Before we complete this subsection, we would like to introduce the following definition that will be used in the bound-preserving technique.

Definition 2.1. *We say the flux $\widehat{\mathbf{u}c_j}$ is consistent with $\hat{\mathbf{u}}$ if $\widehat{\mathbf{u}c_j} = \hat{\mathbf{u}}$ by taking $c_j = 1$ in Ω.*

The numerical flux $\widehat{\mathbf{u}c_j}$ in (2.8) is consistent with the flux $\hat{\mathbf{u}}$ in (2.7), and this is required by the bound-preserving technique.

Remark 2.1. *There are plenty of fluxes can be used following the procedures introduced in the next section. The proofs are basically the same with some minor changes, so we only list some of them below without more details.*

- $\hat{\mathbf{u}} = \mathbf{u}^-$, $\hat{p} = p^+$, $\widehat{\mathbf{u}c_j} = \mathbf{u}^- c_j^- - \alpha[c_j]\mathbf{n}_e$.
- $\hat{\mathbf{u}} = \frac{1}{2}(\mathbf{u}^+ + \mathbf{u}^-)$, $\hat{p} = \frac{1}{2}(p^+ + p^-)$, $\widehat{\mathbf{u}c_j} = \frac{1}{2}(\mathbf{u}^+ c_j^+ + \mathbf{u}^- c_j^-) - \alpha[c_j]\mathbf{n}_e$.

3 Second-order bound-preserving scheme

In this section, we will construct second-order bound-preserving DG scheme with Euler forward time discretization on triangular meshes. For simplicity, we only discuss the technique for cells away from $\partial\Omega$, while the boundary cells can be analyzed following the same lines with some minor changes. A similar analysis for the boundary cells can be found in [16]. We use o_K for the numerical approximation of o in K with cell average $\bar{o}_K$. Moreover, we use o^n as the solution o at time level n. Now, we will demonstrate the bound-preserving technique in detail. For simplicity, we will drop the subindex j in (2.6) and use r, c, $\check{c}$, z for r_j, c_j, $\check{c}_j$, z_j, respectively.

In (2.6), we take $\zeta = 1$ in K to obtain the equation satisfied by the cell average of r

$$\bar{r}_K^{n+1} = H_K^c(r, \boldsymbol{u}, c) + H_K^d(r, \boldsymbol{u}, c) + H_K^s(r, \check{c}, q, z, p) \tag{3.1}$$

where

$$H_K^c(r, \boldsymbol{u}, c) = \frac{1}{3}\bar{r}_K^n - \lambda \sum_{i=1}^{3} \int_{e_K^i} \widehat{\boldsymbol{u}c} \cdot \boldsymbol{\nu}_i ds, \tag{3.2}$$

$$H_K^d(r, \boldsymbol{u}, c) = \frac{1}{3}\bar{r}_K^n + \lambda \sum_{i=1}^{3} \int_{e_K^i} \left(\{\boldsymbol{D}(\boldsymbol{u})\nabla c \cdot \boldsymbol{\nu}_i\} + \frac{\tilde{\alpha}}{\ell_K^i}[c]\mathbf{n}_e \cdot \boldsymbol{\nu}_i \right) ds, \tag{3.3}$$

$$H_K^s(r, \check{c}, q, z, p) = \frac{1}{3}\bar{r}_K^n + \triangle t \overline{\check{c}q - rzp_t}, \tag{3.4}$$

with $\lambda = \frac{\triangle t}{|K|}$ being the ratio of the time step and the area of triangle K, and $\overline{\check{c}q - rzp_t}$ being the cell average of $\check{c}q - rzp_t$. We denote V_i, $i = 1, 2, 3$ as the three vertices of cell K. In this section, we will construct the bound-preserving technique in K, hence for any $w \in W_h$, we define $w(V_i)$ to be the limit evaluated in K. We use the (k+1)-point Gaussian quadrature to approximate the integrals along the cell interfaces in (3.2)-(3.4), and denote $x_{i,\beta}$, $\beta = 1, 2, \cdots, k+1$ as the quadrature points on e_K^i with w_β as the corresponding weights on the reference interval $[-\frac{1}{2}, \frac{1}{2}]$. Moreover, we use quadratures discussed in [47] to compute the cell average $\bar{r}_K^n$. The quadrature contains $L = 3(N_G - 2)(k+1)$ quadrature points, denoted as x_γ, lying in the interior of K with $2N_G - 3 \geq k$, and the quadratures points on the cell interfaces are exactly the $k+1$ Gaussian quadratures points. We denote the quadrature weights corresponding to the interior quadrature points as $\tilde{w}_\gamma$ and those on the cell interfaces as $\hat{w}_\beta$. In [47], it was shown that $\hat{w}_\beta = \frac{2}{3} w_\beta \hat{w}$, where $\hat{w}$ is the quadrature weight corresponding to the first quadrature point in the N_G-point Gauss-Lobatto quadrature on the interval $[-\frac{1}{2}, \frac{1}{2}]$. Based on the above notations, we define the values of o ($o = r, c, p, q, \Phi$) at the quadrature points as $o_K^{i,\beta} = o(x_{i,\beta})$ along the boundary of K and $o_K^\gamma = o(x_\gamma)$ in cell K. Now, we can demonstrate the bound-preserving techniques. We will consider the source term H_K^s first, and discuss the high-order bound-preserving technique.

Lemma 3.1. *Suppose $r^n > 0$ ($c^n > 0$), then $H_K^s(r, \check{c}, q, z, p) > 0$ under the conditions*

$$\triangle t \leq \frac{1}{6zp_M}, \quad \triangle t \leq \frac{\Phi_m}{6q_M}, \tag{3.5}$$

where

$$p_M = \max_{i,\beta,\gamma}((p_t)_K^{i,\beta}, (p_t)_K^\gamma, 0) \quad \Phi_m = \min_x \Phi(x), \quad q_M = \max_{i,\beta,\gamma}\left\{-q_K^{i,\beta}, -q_K^\gamma, 0\right\}. \tag{3.6}$$

Proof. We can write H_K^s as

$$H_K^s(r,\check{c},q,z,p) = \left(\frac{1}{6}\bar{r}_K^n - \triangle t\overline{rzp_t}\right) + \left(\frac{1}{6}\bar{r}_K^n + \triangle t\overline{\check{c}q}\right) := L_1 + L_2.$$

Applying the quadrature in [47], we have

$$\begin{aligned}
L_1 &= \frac{1}{6}\bar{r}_K^n - \triangle t\overline{rzp_t} \\
&= \frac{1}{6}\left(\sum_{i=1}^{3}\sum_{\beta=1}^{k+1}\hat{w}_\beta r_K^{i,\beta} + \sum_{\gamma=1}^{L}\tilde{w}_\gamma r_K^\gamma\right) - \triangle tz\left(\sum_{i=1}^{3}\sum_{\beta=1}^{k+1}\hat{w}_\beta r_K^{i,\beta}(p_t)_K^{i,\beta} + \sum_{\gamma=1}^{L}\tilde{w}_\gamma r_K^\gamma (p_t)_K^\gamma\right) \\
&= \sum_{i=1}^{3}\sum_{\beta=1}^{k+1}\hat{w}_\beta\left(\frac{1}{6} - \triangle tz(p_t)_K^{i,\beta}\right) r_K^{i,\beta} + \sum_{\gamma=1}^{L}\tilde{w}_\gamma\left(\frac{1}{6} - \triangle tz(p_t)_K^\gamma\right) r_K^\gamma.
\end{aligned}$$

Then $L_1 > 0$ under the condition (3.5). We apply the same quadrature for L_2 to obtain

$$\begin{aligned}
L_2 =& \frac{1}{6}\left(\sum_{i=1}^{3}\sum_{\beta=1}^{k+1}\hat{w}_\beta r_K^{i,\beta} + \sum_{\gamma=1}^{L}\tilde{w}_\gamma r_K^\gamma\right) + \triangle t\left(\sum_{i=1}^{3}\sum_{\beta=1}^{k+1}\hat{w}_\beta \check{c}_K^{i,\beta} q_K^{i,\beta} + \sum_{\gamma=1}^{L}\tilde{w}_\gamma \check{c}_K^\gamma q_K^\gamma\right) \\
=& \sum_{i=1}^{3}\sum_{\beta=1}^{k+1}\hat{w}_\beta\left(\frac{1}{6}r_K^{i,\beta} + \triangle t\check{c}_K^{i,\beta} q_K^{i,\beta}\right) + \sum_{\gamma=1}^{L}\tilde{w}_\gamma\left(\frac{1}{6}r_K^\gamma + \triangle t\check{c}_K^\gamma q_K^\gamma\right).
\end{aligned}$$

Notice that $\check{c} = r/\Phi$ if $q < 0$ while $\check{c} > 0$ if $q > 0$. Therefore, under the condition (3.5), each term in the summation above is positive. □

In the rest part of this section, we will consider second-order scheme only, i.e. $k = 1$, $N = 2$, $L = 0$, then $\hat{w} = \frac{1}{2}$ and $w_\beta = 3\hat{w}_\beta$. Now we can analyze the convection term H_K^c and the result is given below.

Lemma 3.2. *Suppose $r^n > 0$ ($c^n > 0$), if α satisfies*

$$\alpha > \max_{i,\beta}\{|\boldsymbol{u}_{K_i}^{i,\beta}|, 0\}, \tag{3.7}$$

and the time step satisfies

$$\Delta t \le \min_{i,\beta}\left\{\frac{1}{9\ell_K^i\alpha}, \frac{1}{9\ell_K^i(|\boldsymbol{u}_K^{i,\beta}| + \alpha)}\right\}\Phi_m|K|. \tag{3.8}$$

we have $H_K^c(r,\boldsymbol{u},c) > 0$.

Proof. Following the same analysis for the source term, we write

$$H_K^c = \sum_{i=1}^{3}\sum_{\beta=1}^{2} w_\beta H_{i,\beta}^c, \quad H_{i,\beta}^c = \frac{1}{9}r_K^{i,\beta} - \lambda\ell_K^i\widehat{\boldsymbol{u}c}^{i,\beta}\cdot\boldsymbol{\nu}_i.$$

We only need to show $H^c_{i,\beta} > 0$.
Case 1: $\boldsymbol{\nu}_i = \mathbf{n}_e$, i.e. $\boldsymbol{u}^- = \boldsymbol{u}_K$, $\boldsymbol{u}^+ = \boldsymbol{u}_{K_i}$, $c^- = c_K$ and $c^+ = c_{K_i}$. Then

$$H^c_{i,\beta} = \frac{1}{9} r^{i,\beta}_K - \lambda \ell^i_K (\boldsymbol{u}^{i,\beta}_{K_i} c^{i,\beta}_{K_i} \cdot \boldsymbol{\nu}_i - \alpha c^{i,\beta}_{K_i} + \alpha c^{i,\beta}_K).$$

Since r and c are both linear functions, we can write the function values of r and c as the interpolation of the values at vertices $\{V_1, V_2, V_3\}$ of K, i.e. for any point x_ρ in K,

$$r^\rho_K = \mu^\rho_1 r_K(V_1) + \mu^\rho_2 r_K(V_2) + \mu^\rho_3 r_K(V_3), \quad c^\rho_K = \mu^\rho_1 c_K(V_1) + \mu^\rho_2 c_K(V_2) + \mu^\rho_3 c_K(V_3), \tag{3.9}$$

with $\mu^\rho_m \geq 0$, $m = 1, 2, 3$, and $\sum_{m=1}^{3} \mu^\rho_m = 1$. Then

$$\begin{aligned} H^c_{i,\beta} &= \sum_{m=1}^{3} \mu^{i,\beta}_m \left(\frac{1}{9} r_K(V_m) - \lambda \ell^i_K \alpha c_K(V_m) \right) + \lambda \ell^i_K (\alpha - \boldsymbol{u}^{i,\beta}_{K_i} \cdot \boldsymbol{\nu}_i) c^{i,\beta}_{K_i} \\ &= \sum_{m=1}^{3} \mu^{i,\beta}_m \left(\frac{1}{9} \Phi_K(V_m) - \lambda \ell^i_K \alpha \right) c_K(V_m) + \lambda \ell^i_K (\alpha - \boldsymbol{u}^{i,\beta}_{K_i} \cdot \boldsymbol{\nu}_i) c^{i,\beta}_{K_i}. \end{aligned}$$

Then we have $H^c_{i,\beta} > 0$, if α and Δt satisfy (3.7) and (3.8), respectively.
Case 2: $\boldsymbol{\nu}_i = -\mathbf{n}_e$, i.e. $\boldsymbol{u}^+ = \boldsymbol{u}_K$, $\boldsymbol{u}^- = \boldsymbol{u}_{K_i}$, $c^+ = c_K$ and $c^- = c_{K_i}$. Then

$$H^c_{i,\beta} = \frac{1}{9} r^{i,\beta}_K - \lambda \ell^i_K (\boldsymbol{u}^{i,\beta}_K c^{i,\beta}_K \cdot \boldsymbol{\nu}_i - \alpha c^{i,\beta}_{K_i} + \alpha c^{i,\beta}_K).$$

Applying (3.9) again, we have

$$H^c_{i,\beta} = \sum_{m=1}^{3} \mu_m \left(\frac{1}{9} \Phi_K(V_m) - \lambda \ell^i_K \mathbf{u}^{i,\beta}_K \cdot \boldsymbol{\nu}_i - \lambda \ell^i_K w_\beta \alpha \right) c_K(V_m) + \lambda \ell^i_K \alpha c^{i,\beta}_{K_i}.$$

Then we have $H^c_{i,\beta} > 0$ under the condition (3.8). □

Finally, we discuss the diffusion part. We also take $k = 1$, $N = 2$, $L = 0$ and the result is given in the following lemma.

Lemma 3.3. *Assume the minimum angle of each triangle K is uniformly bounded away from zero. Suppose $r^n > 0$ ($c^n > 0$), then $H^d_K(r, \boldsymbol{u}, c) > 0$ under the conditions*

$$\tilde{\alpha} \geq \frac{(3 + \sqrt{3})\Lambda}{2 \min_{K,i,j} \left(\sin \left(\theta^{i,j}_K \right) \right)}, \tag{3.10}$$

and

$$\Delta t \leq \frac{\Phi_m |K|}{18 \tilde{\alpha}}, \quad \frac{\triangle t}{|K|} \frac{(3 + \sqrt{3})\Lambda}{\min_{K,i,j} \left(\sin \left(\theta^{i,j}_K \right) \right)} \leq \frac{1}{54} \Phi_m, \tag{3.11}$$

where $\theta^{i,j}_K, i, j = 1, 2, 3, i \neq j$ denotes the angle between the edge e^i_K and e^j_K, and Λ is the largest absolute value of the eigenvalue of $\mathbf{D}$.

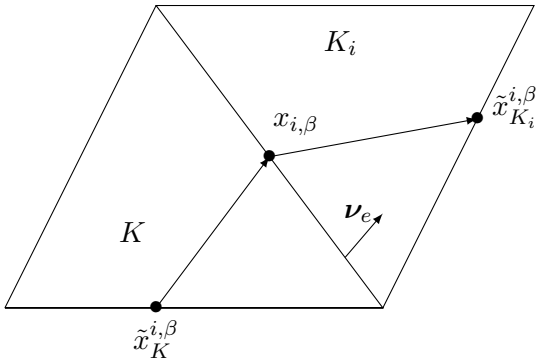

Figure 1: Two intersection points for the numerical flux in diffusion part on the triangular mesh.

Proof. First, we will consider the term

$$\int_{e_K^i} \left(\{\boldsymbol{D}(\boldsymbol{u})\nabla c \cdot \boldsymbol{\nu}_i\} + \frac{\tilde{\alpha}}{\ell_K^i}[c]\mathbf{n}_e \cdot \boldsymbol{\nu}_i \right) ds.$$

Following [48], we write

$$\boldsymbol{D}(\boldsymbol{u})\nabla c \cdot \boldsymbol{\nu}_i = \nabla c \cdot \boldsymbol{D}(\boldsymbol{u})\boldsymbol{\nu}_i = \frac{\partial c}{\partial \boldsymbol{\eta}_i}\|\tilde{\boldsymbol{\eta}}_i\|,$$

where

$$\tilde{\boldsymbol{\eta}}_i = \boldsymbol{D}(\boldsymbol{u})\boldsymbol{\nu}_i, \;\; \boldsymbol{\eta}_i = \frac{\tilde{\boldsymbol{\eta}}_i}{\|\tilde{\boldsymbol{\eta}}_i\|}.$$

Define $\boldsymbol{\eta}_K = \boldsymbol{\eta}_i|_K$ and $\boldsymbol{\eta}_{K_i} = \boldsymbol{\eta}_i|_{K_i}$. Likewise for $\tilde{\boldsymbol{\eta}}_K$ and $\tilde{\boldsymbol{\eta}}_{K_i}$. For each quadrature point $x_{i,\beta}$ on the edge e_K^i, we can draw a straight line from $x_{i,\beta}$ with direction $\boldsymbol{\eta}_{K_i}$ intersects ∂K_i at $\tilde{x}_{K_i}^{i,\beta}$. Similarly, we can draw another straight line from $x_{i,\beta}$ with direction $-\boldsymbol{\eta}_K$ intersects ∂K at $\tilde{x}_K^{i,\beta}$. See Figure 1 for an illustration. It is easy to verify that at $x = x_{i,\beta}$

$$\begin{aligned}
\{\boldsymbol{D}(\boldsymbol{u})\nabla c \cdot \boldsymbol{\nu}_i\} + \frac{\tilde{\alpha}}{\ell_K^i}[c]\mathbf{n}_e \cdot \boldsymbol{\nu}_i &= \frac{1}{2}\boldsymbol{D}(\boldsymbol{u}_K)\nabla c_K \cdot \boldsymbol{\nu}_i + \frac{1}{2}\boldsymbol{D}(\boldsymbol{u}_{K_i})\nabla c_{K_i} \cdot \boldsymbol{\nu}_i + \tilde{\alpha}\frac{(c_{K_i} - c_K)}{\ell_K^i} \\
&= \frac{1}{2}\frac{c_K^{i,\beta} - c(\tilde{x}_K^{i,\beta})}{\|x_K^{i,\beta} - \tilde{x}_K^{i,\beta}\|}\|\tilde{\boldsymbol{\eta}}_K\| + \frac{1}{2}\frac{c(\tilde{x}_{K_i}^{i,\beta}) - c_{K_i}^{i,\beta}}{\|\tilde{x}_{K_i}^{i,\beta} - x_{K_i}^{i,\beta}\|}\|\tilde{\boldsymbol{\eta}}_{K_i}\| + \frac{\tilde{\alpha}}{\ell_K^i}(c_{K_i}^{i,\beta} - c_K^{i,\beta}) \\
&= \left(\frac{\|\tilde{\boldsymbol{\eta}}_K\|}{2\|x_K^{i,\beta} - \tilde{x}_K^{i,\beta}\|} - \frac{\tilde{\alpha}}{\ell_K^i} \right) c_K^{i,\beta} + \left(\frac{\tilde{\alpha}}{\ell_K^i} - \frac{\|\tilde{\boldsymbol{\eta}}_{K_i}\|}{2\|\tilde{x}_{K_i}^{i,\beta} - x_{K_i}^{i,\beta}\|} \right) c_{K_i}^{i,\beta} \\
&\quad - \frac{\|\tilde{\boldsymbol{\eta}}_K\|}{2\|x_K^{i,\beta} - \tilde{x}_K^{i,\beta}\|}c(\tilde{x}_K^{i,\beta}) + \frac{\|\tilde{\boldsymbol{\eta}}_{K_i}\|}{2\|\tilde{x}_{K_i}^{i,\beta} - x_{K_i}^{i,\beta}\|}c(\tilde{x}_{K_i}^{i,\beta}).
\end{aligned}$$

We write the cell average $\bar{r}_K^n$ as

$$\bar{r}_K^n = \sum_{i=1}^{3}\sum_{\beta=1}^{2} \hat{w}_\beta r_K^{i,\beta} = \sum_{i=1}^{3}\sum_{\beta=1}^{2}\sum_{m=1}^{3} \hat{w}_\beta \mu_m^{i,\beta} \Phi_K(V_m) c_K(V_m).$$

we can rewrite $H_K^d(r,\boldsymbol{u},c)$ as

$$\begin{aligned}
H_K^d &= \frac{1}{3}\sum_{i=1}^{3}\sum_{\beta=1}^{2}\sum_{m=1}^{3}\hat{w}_\beta\mu_m^{i,\beta}\Phi_K(V_m)c_K(V_m) + \lambda\sum_{i=1}^{3}\ell_K^i\sum_{\beta=1}^{2}w_\beta\left[\{\boldsymbol{D}(\boldsymbol{u})\nabla c\cdot\boldsymbol{\nu}_i\} + \frac{\tilde{\alpha}}{\ell_K^i}[c]\mathbf{n}_e\cdot\boldsymbol{\nu}_i\right]_{x=x_{i,\beta}}\\
&= \sum_{i=1}^{3}\sum_{\beta=1}^{2}w_\beta\left(\frac{1}{9}\sum_{m=1}^{3}\mu_m^{i,\beta}\Phi_K(V_m)c_K(V_m) + \lambda\ell_K^i\left[\{\boldsymbol{D}(\boldsymbol{u})\nabla c\cdot\boldsymbol{\nu}_i\} + \frac{\tilde{\alpha}}{\ell_K^i}[c]\mathbf{n}_e\cdot\nu_i\right]_{x=x_{i,\beta}}\right)\\
&:= \sum_{i=1}^{3}\sum_{\beta=1}^{2}w_\beta L_{i,\beta} + L,
\end{aligned}$$

where

$$\begin{aligned}
L_{i,\beta} =& \frac{1}{18}\sum_{m=1}^{3}\mu_m^{i,\beta}\Phi_K(V_m)c_K(V_m) + \lambda\ell_K^i\left[\left(\frac{\|\tilde{\boldsymbol{\eta}}_K\|}{2\|x_K^{i,\beta}-\tilde{x}_K^{i,\beta}\|} - \frac{\tilde{\alpha}}{\ell_K^i}\right)c_K^{i,\beta} + \left(\frac{\tilde{\alpha}}{\ell_K^i} - \frac{\|\tilde{\boldsymbol{\eta}}_{K_i}\|}{2\|\tilde{x}_{K_i}^{i,\beta}-x_{K_i}^{i,\beta}\|}\right)c_{K_i}^{i,\beta}\right.\\
&\left. + \frac{\|\tilde{\boldsymbol{\eta}}_{K_i}\|}{2\|\tilde{x}_{K_i}^{i,\beta}-x_{K_i}^{i,\beta}\|}c(\tilde{x}_{K_i}^{i,\beta})\right],\\
L =& \frac{1}{6}\bar{r}_K^n - \lambda\sum_{i=1}^{3}\sum_{\beta=1}^{2}\frac{\ell_K^i\|\tilde{\boldsymbol{\eta}}_K\|}{2\|x_K^{i,\beta}-\tilde{x}_K^{i,\beta}\|}c(\tilde{x}_K^{i,\beta}).
\end{aligned}$$

We need to make $L_{i,\beta} > 0$. In fact

$$\begin{aligned}
L_{i,\beta} =& \frac{1}{18}\sum_{m=1}^{3}\mu_m^{i,\beta}\Phi_K(V_m)c_K(V_m) + \lambda\ell_K^i\left(\frac{\|\tilde{\boldsymbol{\eta}}_K\|}{2\|x_K^{i,\beta}-\tilde{x}_K^{i,\beta}\|} - \frac{\tilde{\alpha}}{\ell_K^i}\right)c_K^{i,\beta}\\
&+ \lambda\ell_K^i\left(\frac{\tilde{\alpha}}{\ell_K^i} - \frac{\|\tilde{\boldsymbol{\eta}}_{K_i}\|}{2\|\tilde{x}_{K_i}^{i,\beta}-x_{K_i}^{i,\beta}\|}\right)c_{K_i}^{i,\beta} + \lambda\ell_K^i\frac{\|\tilde{\boldsymbol{\eta}}_{K_i}\|}{2\|\tilde{x}_{K_i}^{i,\beta}-x_{K_i}^{i,\beta}\|}c(\tilde{x}_{K_i}^{i,\beta})\\
=& \sum_{m=1}^{3}\mu_m^{i,\beta}\left(\frac{1}{18}\Phi_K(V_m) + \lambda\ell_K^i\left(\frac{\|\tilde{\boldsymbol{\eta}}_K\|}{2\|x_K^{i,\beta}-\tilde{x}_K^{i,\beta}\|} - \frac{\tilde{\alpha}}{\ell_K^i}\right)\right)c_K(V_m)\\
&+ \lambda\ell_K^i\left(\frac{\tilde{\alpha}}{\ell_K^i} - \frac{\|\tilde{\boldsymbol{\eta}}_{K_i}\|}{2\|\tilde{x}_{K_i}^{i,\beta}-x_{K_i}^{i,\beta}\|}\right)c_{K_i}^{i,\beta} + \lambda\ell_K^i\frac{\|\tilde{\boldsymbol{\eta}}_{K_i}\|}{2\|\tilde{x}_{K_i}^{i,\beta}-x_{K_i}^{i,\beta}\|}c(\tilde{x}_{K_i}^{i,\beta}).
\end{aligned}$$

Notice that $\|\tilde{\boldsymbol{\eta}}\| \le \Lambda$. To make $L_{i,\beta} > 0$, we need

$$\tilde{\alpha} \ge \frac{\ell_K^i\Lambda}{2\|\tilde{x}_{K_i}^{i,\beta}-x_{K_i}^{i,\beta}\|}, \quad \lambda\ell_K^i\left(\frac{\tilde{\alpha}}{\ell_K^i} - \frac{\|\tilde{\boldsymbol{\eta}}_K\|}{2\|x_K^{i,\beta}-\tilde{x}_K^{i,\beta}\|}\right) \le \frac{1}{18}\Phi_K(V_m).$$

It is easy to compute that

$$\frac{\ell_K^i}{\|\tilde{x}_K^{i,\beta}-x_K^{i,\beta}\|} \le \frac{6}{(3-\sqrt{3})\min_j\sin\left(\theta_K^{i,j}\right)}.$$

and we conclude $L_{i,\beta} > 0$ under the conditions (3.10) and (3.11). Finally, we can apply the same idea above to estimate L. Similar to (3.9), we write

$$c(\tilde{x}_K^{i,\beta}) = \sum_{m=1}^{3} \tilde{\mu}_m^{i,\beta} c_K(V_m),$$

with $0 \le \tilde{\mu}_m^{i,\beta} \le 1$ and $\sum_{m=1}^{3} \tilde{\mu}_m^{i,\beta} = 1$. Then

$$\begin{aligned} L =& \frac{1}{6}\bar{r}_K^n - \lambda \ell_K^i \sum_{i=1}^{3}\sum_{\beta=1}^{2} \frac{\|\tilde{\boldsymbol{\eta}}_K\|}{2\|x_K^{i,\beta} - \tilde{x}_K^{i,\beta}\|} c(\tilde{x}_K^{i,\beta}) \\ =& \sum_{m=1}^{3} \left(\frac{1}{18}\Phi_K(V_m) - \lambda \ell_K^i \sum_{i=1}^{3}\sum_{\beta=1}^{2} \frac{\|\tilde{\boldsymbol{\eta}}_K\| \tilde{\mu}_K^{i,\beta}}{2\|x_K^{i,\beta} - \tilde{x}_K^{i,\beta}\|} \right) c_K(V_m) \\ \ge& \sum_{m=1}^{3} \left(\frac{1}{18}\Phi_K(V_m) - \lambda \sum_{i=1}^{3}\sum_{\beta=1}^{2} \frac{(3+\sqrt{3})\Lambda}{2\min_j \sin\left(\theta_K^{i,j}\right)} \right) c_K(V_m) \end{aligned}$$

Therefore, we have $L > 0$ under the condition (3.11). □

Base on the above three lemmas, we can state the following theorem.

Theorem 3.4. *Suppose $r^n > 0$ ($c^n > 0$), and the parameters α and $\tilde{\alpha}$ satisfy* (3.7) *and* (3.10), *respectively. Then $\bar{r}^{n+1} > 0$ under the conditions* (3.5), (3.8) *and* (3.11).

Now, we have proved $\bar{r}_j > 0$ for $j = 1, 2, \cdots, N-1$. To obtain $\bar{r}_N > 0$, we need to subtract (2.6) from (2.4) to obtain

$$\begin{aligned} (r_{N_t}, \zeta) =& (\boldsymbol{u}c_N - \boldsymbol{D}(\boldsymbol{u})\nabla c_N, \nabla\zeta) + (\check{c}_N q - r_N z_N p_t, \zeta) + \sum_{e\in\Gamma_0} \int_e \widehat{\boldsymbol{u}c_N} \cdot \boldsymbol{n}_e[\zeta] ds \\ & - \sum_{e\in\Gamma_0} \int_e \left(\{\boldsymbol{D}(\boldsymbol{u})\nabla c_N \cdot \boldsymbol{n}_e\}[\zeta] + \{\boldsymbol{D}(\boldsymbol{u})\nabla\zeta \cdot \boldsymbol{n}_e\}[c_N] + \frac{\tilde{\alpha}}{|e|}[c_N][\zeta] \right) ds. \end{aligned} \tag{3.12}$$

Here, we have used the fact that the flux for (2.6) is consistent with that in (2.4). We can observe that the above equation is similar to (2.6). Therefore, following the same analysis above with minor changes we have the following theorem.

Theorem 3.5. *Suppose $0 \le r^n \le \Phi$, and the conditions in Theorem* 3.4 *are satisfied. Moreover, if the fluxes $\widehat{\boldsymbol{u}c_j}$ and $\hat{\boldsymbol{u}}$ are consistent, then $\bar{r}^{n+1} \le \bar{\Phi}$, under the condition*

$$\triangle t \le \frac{1}{6 z_M p_M}, \tag{3.13}$$

where p_M is given in (3.6) *and $z_M = \max\limits_{1\le j\le N} z_j$.*

4 Bound-preserving technique for high-order scheme

In this section, we will apply the flux limiter to construct high-order bound-preserving technique.

4.1 Flux limiter

We use P^k (k>2) polynomials and write (3.1) as

$$\bar{r}_K^{n+1} = \bar{r}_K^n + \lambda \sum_{i=1}^{3} \hat{F}_{e^i} + \Delta t \bar{s},$$

where

$$\hat{F}_{e^i} = -\int_{e^i} \widehat{\boldsymbol{u}c} \cdot \nu_i ds + \int_{e^i} \left(\{\boldsymbol{D}(\boldsymbol{u}) \nabla c \cdot \nu_i\} + \frac{\tilde{\alpha}}{\ell_K^i}[c] \right) ds, \quad \bar{s} = \overline{\tilde{c}q - rz_1 p_t} \tag{4.1}$$

are high-order flux and source, respectively. In Section 3, we have demonstrated how to treat the source terms. Therefore, we only discuss the modification of the high-order fluxes only. We will apply the flux limiter [19, 32] and combine the high-order flux $\hat{F}_{e^i}$ and the second-order fluxes, which was analyzed in Section 3, denoted as $\hat{f}_{e^i}$. We define the new flux as

$$\tilde{F_{e^i}} = \hat{f}_{e^i} + \theta_{e^i}(\hat{F}_{e^i} - \hat{f}_{e^i}),$$

where θ_{e^i} is a parameter that to be chosen. Then the cell average can be written as

$$\bar{r}_K^{n+1} = \bar{r}_K^n + \lambda \sum_{i=1}^{3} \hat{f}_{e^i} + \lambda \sum_{i=1}^{3} \theta_{e^i}(\hat{F}_{e^i} - \hat{f}_{e^i}) + \Delta t \bar{s} = \bar{r}_L^{n+1} + \lambda \sum_{i=1}^{3} \theta_{e^i}(\hat{F}_{e^i} - \hat{f}_{e^i}),$$

where

$$\bar{r}_L^{n+1} = \bar{r}_K^n + \lambda \sum_{i=1}^{3} \hat{f}_{e^i} + \Delta t \bar{s}$$

is the second order cell average which was proved to be positive if Δt is sufficiently small. Notice that, we need the fluxes in (2.6) and (2.4) to be consistent. Therefore, we have to discuss the fluxes for all components together. We define $\hat{f}_{e^i}^j$ and $\hat{F}_{e^i}^j$ as the second- and high-order fluxes for component j, $j = 1, 2, \cdots, N$, respectively, and the cell average $\bar{r}$ for the jth component to be $\bar{r}_j$. To compute $\hat{f}_{e^i}^j$, we only replace the c_j in $\hat{F}_{e^i}^j$ in (4.1) by a second-order approximation. We cannot change $\mathbf{u}$, since we want $\sum_{j=1}^N \hat{F}_{e^i}^j = \sum_{j=1}^N \hat{f}_{e^i}^j = \hat{\mathbf{u}}_{e^i}$, which due to the flux consistency requirement. To construct the second-order c_j, we can simply apply the second-order L^2 projection to the high-order c_j, and then apply the limiter discussed in 4.2 with $k = 1$ and Φ as the second-order L^2 projection of ϕ. We can choose the parameter θ_{e^i} as follows:

1. For any $K \in \Omega_h$, set $\beta_K = 0$.
2. Define $\hat{F}_{e^i}^N = \hat{\mathbf{u}}_{e^i} - \sum_{j=1}^{N-1} \hat{F}_{e^i}^j$, $\hat{f}_{e^i}^N = \hat{\mathbf{u}}_{e^i} - \sum_{j=1}^{N-1} f_{e^i}^j$ and $\bar{r}_n = \bar{\Phi} - \sum_{j=1}^{N-1} \bar{r}_j$.
3. For any $j = 1, 2, \cdots, N$, if $\hat{F}_{e^i}^j - \hat{f}_{e^i}^j \geq 0$, take $\theta_{K,e^i}^j = 1$, otherwise set $\beta_K = \beta_K + \hat{F}_{e^i}^j - \hat{f}_{e^i}^j$.

4. For those edges e^i with $\hat{F}^j_{e^i} - \hat{f}^j_{e^i} < 0$, we set $\theta^j_{K,e^i} = \min\left\{-\dfrac{\bar{r}^{n+1}_{j,L}}{\lambda\beta^m_K}, 1\right\}$.

5. Take $\theta_{K,e^i} = \min\limits_{1\le j\le N} \theta^j_{K,e^i}$.

6. For any $e \in \Gamma_0$, we can find $K_1, K_2 \in \Omega_h$ such that $K_1 \cap K_2 = e$. We take $\theta_e = \min\{\theta_{K_1,e}, \theta_{K_2,e}\}$.

Following the same analyses in [6], we have $\bar{r}^{n+1}_j \ge 0, j = 1, 2, \cdots, N$. Thus, $0 \le \bar{r}^{n+1}_j \le \bar{\Phi}$, since we have the relationship $\bar{r}^{n+1}_1 + \bar{r}^{n+1}_2 + \ldots + \bar{r}^{n+1}_N = \bar{\Phi}$.

Remark 4.1. *In (2.4)-(2.6), we do not compute r_N (c_N) directly. Step 2 in the above algorithm is used to compute the fluxes in (3.12). Actually, we can simply take $F^N_{e^i} = -\sum_{j=1}^{N-1} F^j_{e^i}$, $\hat{f}^N_{e^i} = -\sum_{j=1}^{N-1} f^j_{e^i}$, since we only need the difference of the higher order and lower order fluxes. Moreover, step 5 is used to construct consistent fluxes (See definition 2.1).*

4.2 Slope limiter

In this section, we discuss the limiters to be applied. As discussed in [16], the traditional slope limiter (1.4) cannot be applied. In this paper, we will construct a new one. We consider problem with 2 components first and then extend it to N-component ones. The algorithm is given as follows.

1. Define $\hat{S} = \{x \in K : r(x) \le 0\}$. Take

$$\hat{r}_1 = r_1 + \theta\left(\frac{\bar{r}_1}{\bar{\Phi}}\Phi - r_1\right), \qquad \theta = \max_{y\in\hat{S}}\left\{\frac{-r_1(y)\bar{\Phi}}{\bar{r}_1\Phi(y) - r_1(y)\bar{\Phi}}, 0\right\}. \tag{4.2}$$

2. Set $r_2 = \Phi - \hat{r}_1$, and repeat the above step for r_2.

3. Take $\tilde{r}_1 = \Phi - \hat{r}_2$ as the new approximation.

Remark 4.2. *In step 1, it is easy to see that $\hat{r}_1 \ge 0$ which further implies $r_2 \le \Phi$. In step 2, we have*

$$\hat{r}_2 = r_2 + \theta\left(\frac{\bar{r}_2}{\bar{\Phi}}\Phi - r_2\right) = (1-\theta)r_2 + \theta\frac{\bar{r}_2}{\bar{\Phi}}\Phi \le (1-\theta)\Phi + \theta\Phi = \Phi, \forall\theta \in [0,1],$$

which means the property $\hat{r}_2 \le \Phi$ is inherited naturally from $r_2 \le \Phi$, no matter which parameter θ is chosen. This fact gives us enough space to modify $\hat{r}_2$ such that $\hat{r}_2 \ge 0$, as we did in step one. Therefore, after step 3, we have $0 \le \tilde{r}_1 \le \Phi$. Besides the above, it is easy to check that the limiter does not change the numerical cell averages, i.e., $\int_K \tilde{r}(x)dx = \int_K r(x)dx$.

Moreover, we can also prove that the limiter does not affect the accuracy.

Theorem 4.1. *Let $R(x) \in C^{k+1}(K)$ and $r(x), \Phi(x) \in P^k(K)$ with $0 \le \bar{r} \le \bar{\Phi}$ and $\|r(x) - R(x)\|_\infty \le Ch^{k+1}$. Assume there exist two positive constants Φ_m and Φ_M such that $0 < \Phi_m \le \Phi(x) \le \Phi_M$, then $\|\tilde{r}(x) - R(x)\|_\infty \le Ch^{k+1}$.*

Proof. WLOG, we assume $\theta > 0$ in (4.2) and need to show the modification in step 1 keeps the accurate :$\|\hat{r}(x) - r(x)\|_\infty \le Ch^{k+1}$. Denote $r_m = \min_{x\in K} r(x), r_M = \max_{x\in K} r(x)$. Let $y \in K$ be the point at which the maximum in (4.2) is achieved and define $r_y = r(y) < 0, \Phi_y = \Phi(y)$. Then

$$\theta = \frac{-r_y}{\frac{\bar{r}}{\bar{\Phi}}\Phi_y - r_y} \le \frac{-r_y}{\bar{r}\frac{\Phi_m}{\Phi_M} - r_y} \le \frac{-r_y}{\bar{r}\frac{\Phi_m}{\Phi_M} - r_y\frac{\Phi_m}{\Phi_M}} = \frac{-r_y}{\bar{r} - r_y}\frac{\Phi_M}{\Phi_m} \le \frac{-r_m}{\bar{r} - r_m}\frac{\Phi_M}{\Phi_m},$$

which further yields

$$|\hat{r} - r| = \theta|\frac{\bar{r}}{\bar{\Phi}}\Phi - r| \le \frac{\Phi_M}{\Phi_m}\frac{-r_m}{\bar{r} - r_m}|\frac{\bar{r}}{\bar{\Phi}}\Phi - r| = \frac{\Phi_M}{\Phi_m}(-r_m)\frac{|\bar{r}\frac{\Phi}{\bar{\Phi}} - r|}{\bar{r} - r_m}.$$

Since $\frac{\Phi_M}{\Phi_m}$ is a constant and $|-r_m| \le Ch^{k+1}$, we only need to prove that $\frac{|\bar{r}\frac{\phi}{\bar{\phi}} - r|}{\bar{r} - r_m} \le C$ for some positive constant C independent of x and h. Notice that

$$\bar{r}\frac{\Phi_m}{\Phi_M} - r_M \le \bar{r}\frac{\Phi}{\bar{\Phi}} - r \le \bar{r}\frac{\Phi_M}{\Phi_m} - r_m,$$

we have

$$\left|\bar{r}\frac{\Phi}{\bar{\Phi}} - r\right| \le \max\left\{\left|\bar{r}\frac{\Phi_M}{\Phi_m} - r_m\right|, \left|\bar{r}\frac{\Phi_m}{\Phi_M} - r_M\right|\right\},$$

which further yields

$$\frac{|\bar{r}\frac{\Phi}{\bar{\Phi}} - r|}{\bar{r} - r_m} \le \max\left\{\frac{|\bar{r}\frac{\Phi_M}{\Phi_m} - r_m|}{\bar{r} - r_m}, \frac{|\bar{r}\frac{\Phi_m}{\Phi_M} - r_M|}{\bar{r} - r_m}\right\}.$$

Next, we will prove the boundedness of $\frac{|\bar{r}\frac{\Phi_M}{\Phi_m} - r_m|}{\bar{r} - r_m}$, and $\frac{|\bar{r}\frac{\Phi_m}{\Phi_M} - r_M|}{\bar{r} - r_m}$, respectively. For the first term, we have

$$\frac{|\bar{r}\frac{\Phi_M}{\Phi_m} - r_m|}{\bar{r} - r_m} = \frac{\bar{r}\frac{\Phi_M}{\Phi_m} - r_m}{\bar{r} - r_m} \le \frac{\bar{r}\frac{\Phi_M}{\Phi_m} - r_m\frac{\Phi_M}{\Phi_m}}{\bar{r} - r_m} = \frac{\Phi_M}{\Phi_m}.$$

while for the second term

$$\frac{|\bar{r}\frac{\Phi_m}{\Phi_M} - r_M|}{\bar{r} - r_m} = -\frac{\bar{r} - r_M + \bar{r}(\frac{\Phi_m}{\Phi_M} - 1)}{\bar{r} - r_m} \le -\frac{\bar{r} - r_M}{\bar{r} - r_m} - \frac{\bar{r}(\frac{\Phi_m}{\Phi_M} - 1)}{\bar{r}} \le \frac{r_M - \bar{r}}{\bar{r} - r_m} + 1 - \frac{\Phi_m}{\Phi_M}.$$

In Appendix C of [45], Zhang proved that for any non-constant polynomial of degree k, say $p(x)$, we have

$$|\frac{\bar{p} - \max p(x)}{\bar{p} - \min p(x)}| \le C_k,$$

where C_k is a constant only depends on the polynomial degree k. Thus,

$$\frac{|\bar{r}\frac{\Phi_m}{\Phi_M} - r_M|}{\bar{r} - r_m} \le C_k + 1 - \frac{\Phi_m}{\Phi_M},$$

and we finish the proof. □

Remark 4.3. *There are two ways to apply this limiter in an N-component system. One way is to compute the parameter θ_j for the jth component, $(j = 1, 2, \cdots, N)$ and then take $\theta = \max_j \theta_j$. Another way is to modify $r_1, r_2, \cdots, r_{N-1}$ one by one such that $r_1 \in [0, \Phi], r_2 \in [0, \Phi - r_1], r_3 \in [0, \Phi - r_1 - r_2], \cdots, r_{N-1} \in [0, \Phi - r_1 - r_2 \cdots - r_{N-2}]$.*

4.3 High-order time discretization

In this section, we extend the Euler forward time discretization to high-order ones which are convex combinations of Euler forwards. In this paper, we use third-order strong stability preserving (SSP) high-order time discretization to solve the ODE system $\mathbf{u_t} = \mathbf{L}(\mathbf{u})$:

$$\begin{aligned}
\mathbf{u}^{(1)} =& \mathbf{u}^n + \Delta t \mathbf{L}(\mathbf{u}, t^n), \\
\mathbf{u}^{(2)} =& \frac{3}{4}\mathbf{u}^n + \frac{1}{4}\left(\mathbf{u}^{(1)} + \Delta t \mathbf{L}(\mathbf{u}^{(1)}, t^{n+1})\right), \\
\mathbf{u}^{n+1} =& \frac{1}{3}\mathbf{u}^n + \frac{2}{3}\left(\mathbf{u}^{(2)} + \Delta t \mathbf{L}(\mathbf{u}^{(2)}, t^n + \frac{\Delta t}{2})\right).
\end{aligned}$$

Another choice is third-order SSP multi-step method:

$$\mathbf{u}^{n+1} = \frac{16}{27}(\mathbf{u}^n + 3\Delta t \mathbf{L}(\mathbf{u}^n, t^n)) + \frac{11}{27}(\mathbf{u}^{n-3} + \frac{12}{11}\Delta t \mathbf{L}(\mathbf{u}^{n-3}, t^{n-3})).$$

More details can be found in [14, 15, 24].

5 Numerical experiments

In this section, we provide numerical experiments to test the accuracy and stability of the high-order bound-preserving DG scheme. In all the examples, we choose $N = 3$, and consider fluid mixture with 3 components. Moreover, we use the third-order SSP Runge-Kutta discretization in time and P^2 element in space. The computational domain is set to be $\Omega = [0, 2\pi] \times [0, 2\pi]$. To construct Ω_h, we first equally divide Ω into $M \times M$ rectangles and the triangles are obtained by equally divide each rectangle into two. See Figure 2 for the mesh.

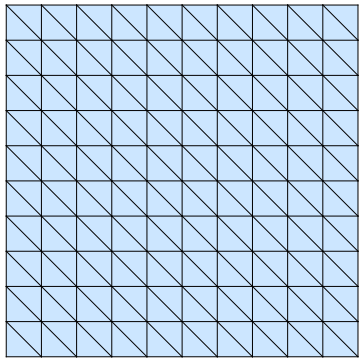

Figure 2: Triangular mesh ($M = 10$)

Example 5.1. *We set the initial conditions as*

$$c_{1,0}(x,y)=\frac{1}{6}(1+\frac{1}{2}(\cos x+\cos y)),\quad c_{2,0}(x,y)=\frac{1}{3}(1+\cos x\cos y),$$
$$c_{3,0}(x,y)=1-c_{1,0}(x,y)-c_{2,0}(x,y),\quad p_0(x,y)=\cos x\cos y-1,$$

and the source variables are taken as

$$\tilde{c}_1(x,y,t)=\frac{1}{6}(1+\frac{1}{2}e^{-\gamma t}(\cos x+\cos y-\frac{1}{2}\sin x\cos y-\frac{1}{2}\sin y\cos x)),$$
$$\tilde{c}_2(x,y,t)=\frac{1}{3}(1+e^{-2\gamma t}(\cos x\cos y-\frac{1}{2}\sin^2 x\cos^2 y-\frac{1}{2}\cos^2 x\sin^2 y)),$$
$$\tilde{c}_3(x,y,t)=1-\tilde{c}_1(x,y,t)-\tilde{c}_2(x,y,t),\qquad q(x,y,t)=2e^{-2t}.$$

Other parameters are chosen as

$$\phi(x,y)=\mu(c_1,c_2)=k(x,y)=a(x,y,c_1,c_2)=z_1=z_2=z_3=1,\quad \boldsymbol{D}(\boldsymbol{u})=diag(\gamma,\gamma).$$

It is easy to verify that the exact solutions are

$$c_1(x,y,t)=\frac{1}{6}(1+\frac{1}{2}e^{-\gamma t}(\cos x+\cos y)),\quad c_2(x,y,t)=\frac{1}{3}(1+e^{-2\gamma t}\cos x\cos y),$$
$$c_3(x,y,t)=1-c_1(x,y,t)-c_2(x,y,t),\quad p(x,y,t)=e^{-2t}(\cos x\cos y-1).$$

In the numerical simulation, we choose $\gamma=0.01$, final time $T=0.01$ and $\Delta t=0.001h^2$ to reduce the time error. The computational results are shown in Table 1, illustrating the L^2 error and convergence orders for c_1 and c_2 with and without bound-preserving technique. From the table, we observe optimal convergence rates. Therefore, the flux limiter and slope limiter do not degenerate the convergence order.

Example 5.2. *We choose the initial conditions as*

$$c_{1,0}(x,y)=\begin{cases}1, & x\le\frac{\pi}{2},y\le\frac{\pi}{2},\\ 0, & otherwise.\end{cases}\qquad c_{2,0}(x,y)=\begin{cases}1, & x\ge\frac{3\pi}{2},y\ge\frac{3\pi}{2},\\ 0, & otherwise.\end{cases}$$

$$c_{3,0}(x,y)=1-c_{1,0}(x,y)-c_{2,0}(x,y)\quad and\quad p_0(x,y)=\cos(\frac{x}{2})+\cos(\frac{y}{2}).$$

Other parameters are taken as

$$z_1=z_2=1,z_3=10,q(x,y,t)=0,\boldsymbol{D}(\boldsymbol{u})=0,$$
$$\mu(c_1,c_2)=k(x,y)=a(x,y,c_1,c_2)=\phi(x,y)=1.$$

	c_1				c_2			
	no limiter		with limiter		no limiter		with limiter	
M	L^2 error	order	L^2 error	order	L^2 error	order	L^2 error	order
5	3.02e-3	–	4.61e-3	–	2.12e-2	–	2.39e-2	–
10	5.00e-4	2.59	5.30e-4	3.12	3.29e-3	2.69	3.47e-3	2.78
20	8.85e-5	2.50	8.86e-5	2.58	5.34e-4	2.63	5.34e-4	2.70
40	1.25e-5	2.82	1.25e-5	2.82	7.25e-5	2.88	7.25e-5	2.88
80	1.71e-6	2.87	1.71e-6	2.87	9.41e-6	2.95	9.41e-6	2.95
160	2.02e-7	3.09	2.02e-7	3.09	1.16e-6	3.02	1.16e-6	3.02

Table 1: Example 5.1: Accuracy test for c_1 and c_2 with and without bound-preserving technique.

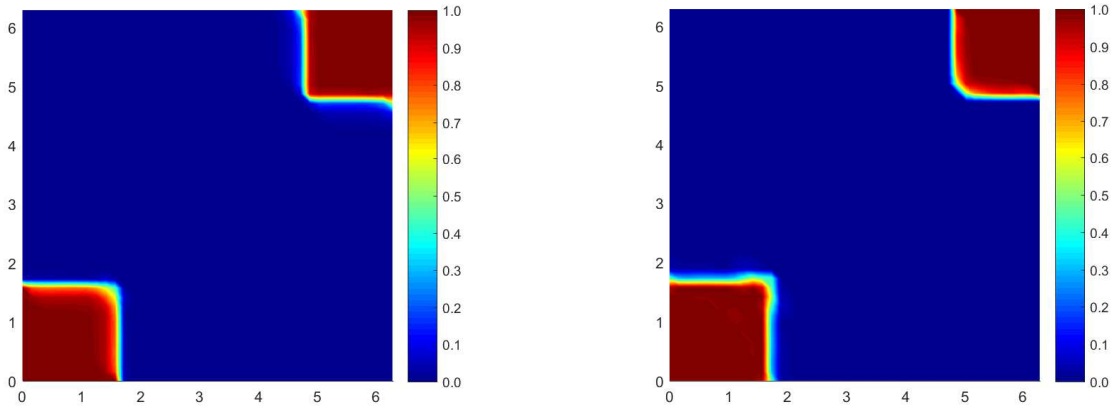

(a) T=0.1 s

(b) T=0.6 s

Figure 3: Example 5.2: Numerical approximations of c_1 and c_2

We use this example to demonstrate the stability of the scheme. We choose $\mathbf{D} = \mathbf{0}$, then the diffusion term will not provide any dissipation to the scheme. We compute the components c_1 and c_2 at time $T = 0.1s$ and $T = 0.6s$, respectively, with $M = 40$ and $\Delta t = 0.001h^2$ ($h = \frac{2\pi}{40}$). The numerical results are shown as Figure 3. From the figure we can see that the concentrations c_1 and c_2 are between 0 and 1. To test the effectiveness of the bound-preserving technique, we simulate the example without the bound-preserving limiters, and the numerical approximations blow up at about $0.003s$ even though we take time step size as small as $\Delta t = 0.0001h^2$. In [16], we demonstrated that the reason for the blow-up of the numerical approximations is the ill-posedness of the system. This example demonstrates the necessity of the bound-preserving technique in solving compressible miscible displacements in porous media.

Example 5.3. *We investigate the displacement of 3-phase porous media flow in the five-spot arrangement of injection and production wells. The computational domain is a square region taken as quarter-of-a-five-spot pattern. The three phases are light oil c_1 (with low viscosity and high compressibility), heavy oil c_2 (with high viscosity and low compressibility) and water c_3 (with medium viscosity and medium compressibility).*
The initial concentrations of oil (water) are

$$c_{1,0}(x,y) = \begin{cases} 1, & x \le \frac{\pi}{2}, y \le \frac{\pi}{2}, \\ 0, & otherwise. \end{cases} \qquad c_{2,0}(x,y) = \begin{cases} 0, & x \le \frac{\pi}{2}, y \le \frac{\pi}{2}, \\ 1, & otherwise. \end{cases} \qquad c_{3,0}(x,y) = 0.$$

Therefore, the lower-left part of the region is light oil enrichment area while the other part is heavy oil enrichment area. Moreover, no water exists initially and the initial pressure is taken as 0 in the whole computational domain. To simulate the random perturbation of porosity and permeability around their average value, we choose the porosity and permeability as

$$\phi(x,y) = 0.5 + 0.05\sin(5x)\sin(5y) \quad \text{and} \quad k(x,y) = 1.0 + 0.1\cos(5x)\cos(5y),$$

respectively. Other parameters are taken as

$$\mu(c_1,c_2,c_3) = 0.4c_1 + 2.0c_2 + 1.0c_3, \quad z_1 = 1.2, \quad z_2 = 0.8, \quad z_3 = 1.0, \quad \mathbf{D} = diag(|\mathbf{u}|,|\mathbf{u}|).$$

The injection well is located in lower-left corner and production well is located in upper-right corner, treated as δ sources.

This example is used for petroleum production simulations. We compute the components c_1 and c_2 at time $T = 0.2, 0.8$ with $M = 35$ and $\Delta t = 0.001h^2 (h = \dfrac{2\pi}{35})$. The distributions of c_1, c_2 and $c_1 + c_2$ at different time are shown in figures 4a-4f, respectively. From the figure we can see that c_1, c_2 and $c_1 + c_2$ are all between 0 and 1.

Example 5.4. *To show the significance of the bound-preserving technique in real petroleum production simulations, we choose the exact parameters in Example 5.3, except $\mathbf{D} = \mathbf{0}$ in order to avoid any dissipation to the scheme which is resulted from the diffusion term.*

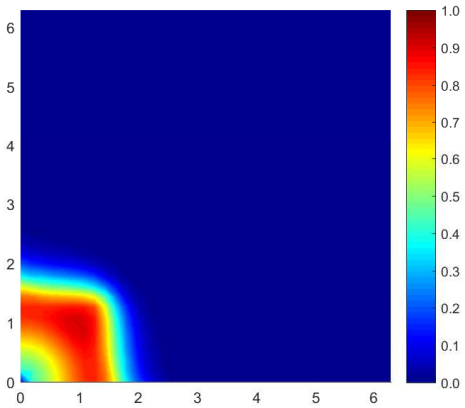

(a) c_1 at T=0.2 s

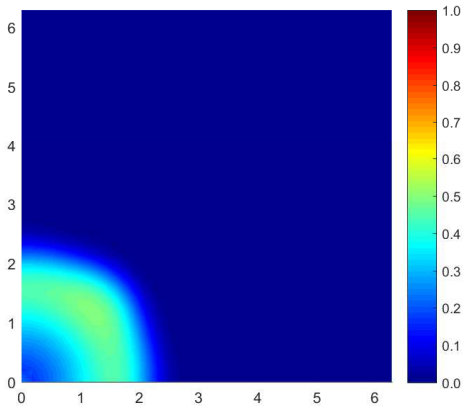

(b) c_1 at T=0.8 s

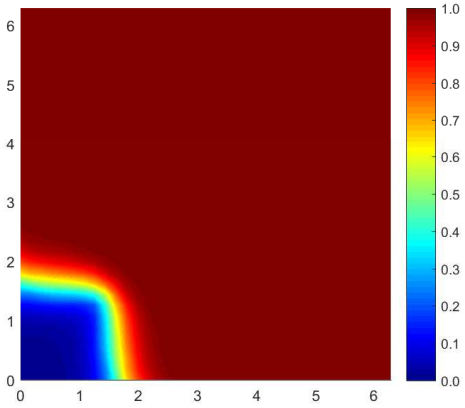

(c) c_2 at T=0.2 s

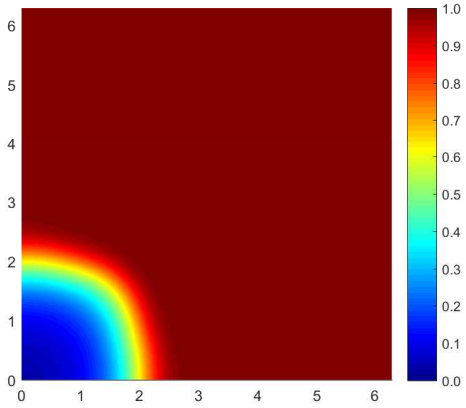

(d) c_2 at T=0.8 s

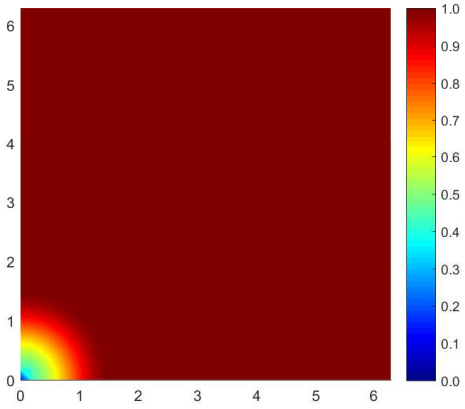

(e) $c_1 + c_2$ at T=0.2 s

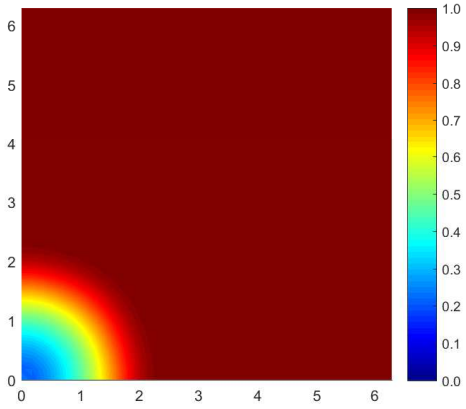

(f) $c_1 + c_2$ at T=0.8 s

Figure 4: Example 5.3: Concentrations of c_1, c_2 and $c_1 + c_2$.

This example is used for petroleum production simulations when diffusion effect is negligible. We compute the components c_1 and c_2 at time $T = 0.2, 0.8$ with $M = 35$ and $\Delta t = 0.001h^2 (h = \frac{2\pi}{35})$. The distributions of c_1, c_2, and c_3 at different time along diagonal $y = x$ are shown in figures 5a-5f, respectively. From the figures we can see that the concentrations c_1, c_2, and c_3 are between 0 and 1.

However, the numerical approximations without bound-preserving limiters blow up at about $T = 0.25$ if we take the same time step as before. The distribution of components along diagonal at time $T = 0.1, 0.2$ are shown in figures 6a-6f, from which we can observe strong oscillations and physically irrelevant values. Further experiments show that, even though we take the time step as small as $\Delta t = 0.0001h^2$, the numerical approximations still blow up at about $T = 0.26$, which implies the necessity of the bound-preserving technique.

6 Concluding remarks

In this paper, we constructed high-order bound-preserving DG methods for compressible miscible displacements in porous media on triangular meshes. We have applied the technique to the problem with multi-component fluid mixtures. Numerical simulations shown the accuracy and necessity of the bound-preserving technique.

References

[1] S. Bartels, M. Jensen and R. Müller, *Discontinuous Galerkin finite element convergence for incompressible miscible displacement problem of low regularity,* SIAM Journal on Numerical Analysis, 47 (2009), 3720-3743.

[2] P. Bastian, *A fully-coupled discontinuous Galerkin method for two-phase flow in porous media with discontinuous capillary pressure,* Computational Geosciences, 18 (2014), 779-796.

[3] H.-Z. Chen and H. Wang, *An optimal-order error estimate on an H^1-Galerkin mixed method for a nonlinear parabolic equation in porous medium flow,* Numerical Methods for Partial Differential Equations, 26 (2010), 188-205.

[4] Z. Chen, H. Huang and J. Yan, *Third order Maximum-principle-satisfying direct discontinuous Galerkin methods for time dependent convection diffusion equations on unstructured triangular meshes,* Journal of Computational Physics, 308 (2016), 198-217.

[5] S.-H. Chou and Q. Li, *Mixed finite element methods for compressible miscible displacement in porous media,* Mathematics of Computation, 57 (1991), 507-527.

[6] A. Christlieb, Y. Liu, Q. Tang and Z. Xu, *Parametrized Maximum-principle-preserving and positivity-preserving flux limiter for WENO schemes on unstructured meshes*, Journal of Computational Physics, 281 (2015), 334-351.

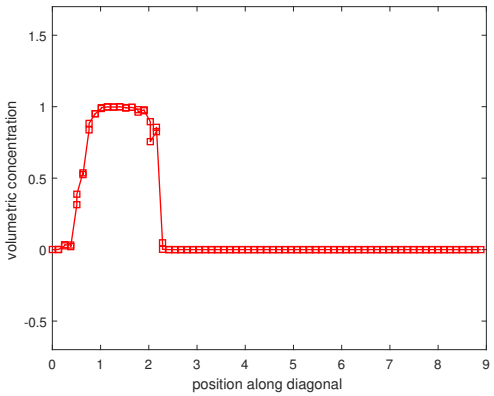

(a) c_1 at T=0.2 s

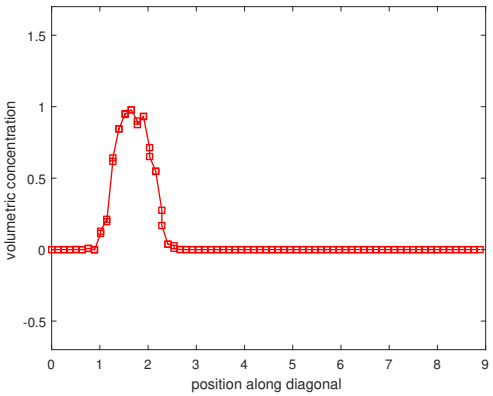

(b) c_1 at T=0.8 s

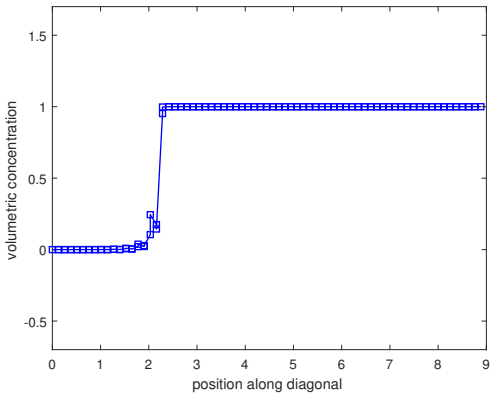

(c) c_2 at T=0.2 s

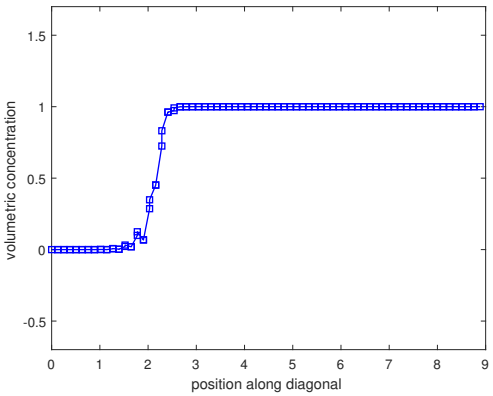

(d) c_2 at T=0.8 s

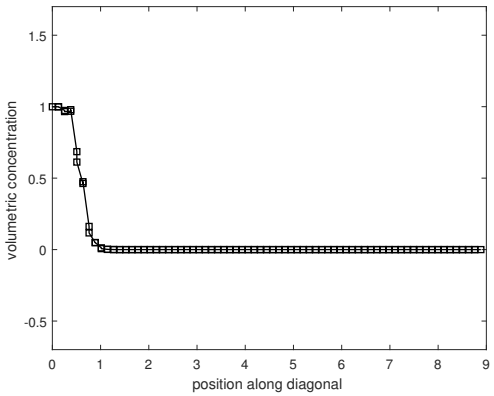

(e) c_3 at T=0.2 s

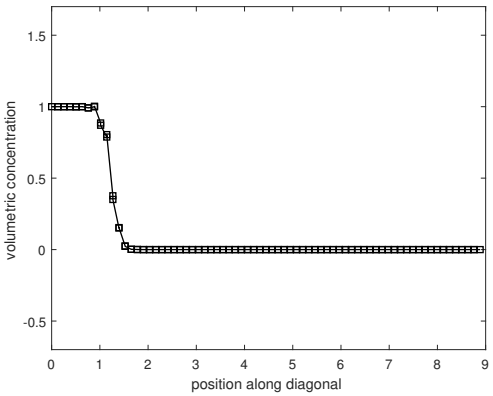

(f) c_3 at T=0.8 s

Figure 5: Example 5.4: Concentrations of c_1, c_2 and c_3 with limiters

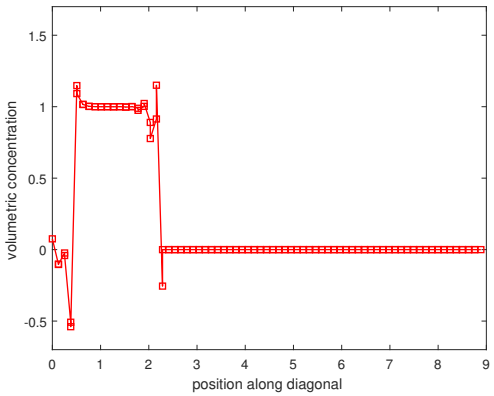

(a) c_1 at T=0.1 s

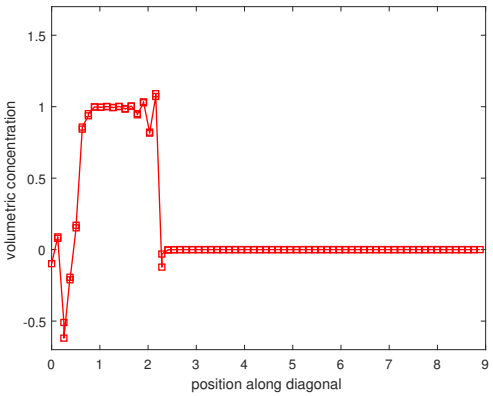

(b) c_1 at T=0.2 s

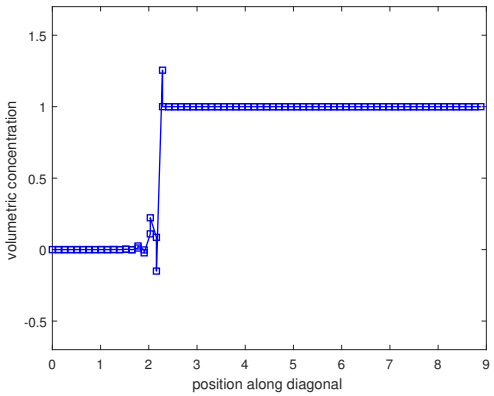

(c) c_2 at T=0.1 s

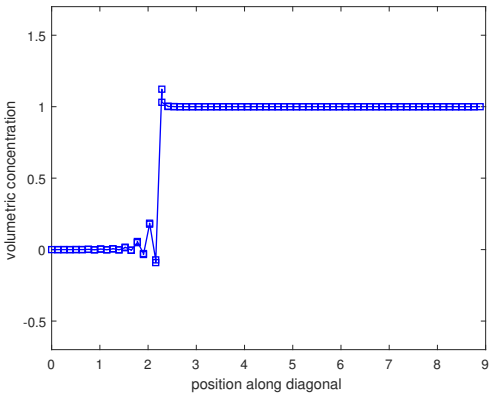

(d) c_2 at T=0.2 s

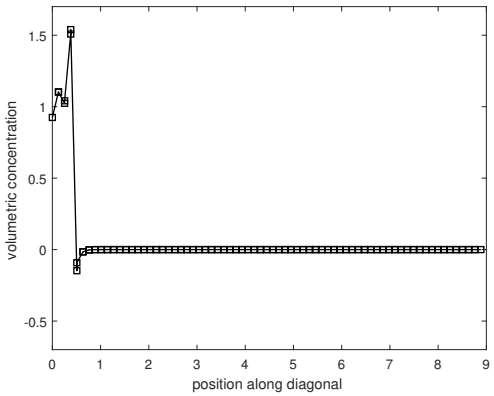

(e) c_3 at T=0.1 s

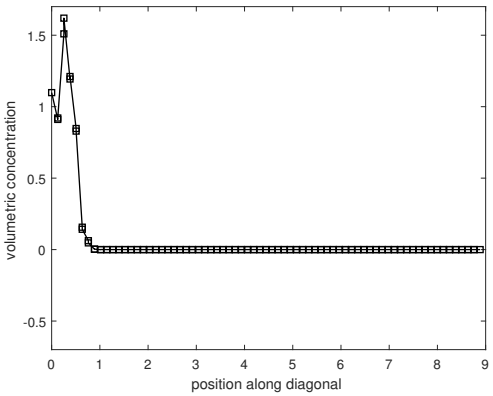

(f) c_3 at T=0.2 s

Figure 6: Example 5.4: Concentrations of c_1, c_2 and c_3 without limiters

[7] M. Cui, *A combined mixed and discontinuous Galerkin method for compressible miscible displacement problem in porous media*, Journal of Computational and Applied Mathematics, 198 (2007), 19-34.

[8] M. Cui, *Analysis of a semidiscrete discontinuous Galerkin scheme for compressible miscible displacement problem*, Journal of Computational and Applied Mathematics, 214 (2008), 617-636.

[9] J. Douglas, Jr., R.E. Ewing and M.F. Wheeler, *A time-discretization procedure for a mixed finite element approximation of miscible displacement in porous media*, R.A.I.R.O. Analyse numérique, 17 (1983), 249-256.

[10] J. Douglas, Jr., R.E. Ewing and M.F. Wheeler, *The approximation of the pressure by a mixed method in the simulation of miscible displacement*, R.A.I.R.O. Analyse numérique, 17 (1983), 17-33.

[11] J. Douglas, Jr. and J. Roberts, *Numerical methods for a model for compressible miscible displacement in porous media,* Mathematics of Computation, 41 (1983), 441-459.

[12] A. Ern, I. Mozolevski and L. Schuh, *Discontinuous Galerkin approximation of two-phase flows in heterogeneous porous media with discontinuous capillary pressures,* Computer Methods in Applied Mechanics and Engineering, 199 (2010), 1491-1501.

[13] A. Ern, I. Mozolevski and L. Schuh, *Accurate velocity reconstruction for Discontinuous Galerkin approximations of two-phase porous media flows,* Comptes Rendus Mathematique, 347 (2009), 551-554.

[14] S. Gottlieb, D. Ketcheson and C.-W. Shu, *High order strong stability preserving time discretizations*, Journal of Scientific Computing, 38 (2009), 251-289.

[15] S. Gottlieb, C.-W. Shu and E. Tadmor, *Strong stability-preserving high-order time discretization methods*, SIAM review 43.1 (2001), pp. 89-112.

[16] H. Guo and Y. Yang, *Bound-Preserving Discontinuous Galerkin Method for Compressible Miscible Displacement in Porous Media*, SIAM Journal on Scientific Computing, 39 (2017), A1969-A1990.

[17] H. Guo and Q. Zhang, *Error analysis of the semi-discrete local discontinuous Galerkin method for compressible miscible displacement problem in porous media*, Applied Mathematics and Computation, 259 (2015), 88-105.

[18] H. Guo, Q. Zhang and Y. Yang, *A combined mixed finite element method and local discontinuous Galerkin method for miscible displacement problem in porous media,* Science China Mathematics, 57 (2014), 2301-2320.

[19] L. Guo and Y. Yang, *Positivity preserving high-order local discontinuous Galerkin method for parabolic equations with blow-up solutions*, Journal of Computational Physics, 289 (2015), 181-195.

[20] S. Kumar, *A mixed and discontinuous Galerkin finite volume element method for incompressible miscible displacement problems in porous media,* Numerical Methods for Partial Differential Equations, 28 (2012), 1354-1381.

[21] N. Ma, D. Yang and T. Lu, *L^2-norm error bounds of characteristics collocation method for compressible miscible displacement in porous media*, International Journal of Numerical Analysis and Modeling, 2 (2005), 28-42.

[22] B. Rivière, *Discontinuous Galerkin finite element methods for solving the miscible displacement problem in porous media,* Ph.D. Thesis, The University of Texas at Austin, 2000.

[23] T. Qin, C.-W. Shu and Y. Yang, *Bound-preserving discontinuous Galerkin methods for relativistic hydrodynamics,* Journal of Computational Physics, 315 (2016), 323-347.

[24] C.-W. Shu, *Total-variation-diminishing time discretizations*, SIAM Journal on Scientific and Statistical Computing 9 (1988), 1073-1084.

[25] S. Sun, B. Rivière and M.F. Wheeler, *A combined mixed finite element and discontinuous Galerkin method for miscible displacement problem in porous media,* Recent Progress in Computational and Applied PDEs, Tony Chan et al. (Eds.), Kluwer Academic Publishers, Plenum Press, Dordrecht, NewYork, 2002, 323-351.

[26] S. Sun and M.F. Wheeler, *Discontinuous Galerkin methods for coupled flow and reactive transport problems,* Applied Numerical Mathematics, 52 (2005), 273-298.

[27] S. Sun and M.F. Wheeler, *Symmetric and nonsymmetric discontinuous Galerkin methods for reactive transport in porous media,* SIAM Journal on Numerical Analysis, 43 (2005), 195-219.

[28] H. Wang, D. Liang, R.E. Ewing, S.L. Lyons and G. Qin, *An approximation to miscible fluid flows in porous media with point sources and sinks by an Eulerian-Lagrangian localized adjoint method and mixed finite element methods,* SIAM Journal on Scentific Computing, 22 (2000), 561-581.

[29] H. Wang, D. Liang, R.E. Ewing, S.L. Lyons and G. Qin, *An accurate approximation to compressible flow in porous media with wells,* Numerical Treatment of Multiphase Flows in Porous Media, Lecture Notes in Physics, 552 (2000), 324-332.

[30] M. F. Wheeler and B. L. Darlow, *Interiori penalty Galerkin methods for miscible displacement problems in porous media,* Computational Methods in Nonlinear Mechanics, North-Holland, Amsterdam, 1980, 458-506.

[31] Y. Xing, X. Zhang and C.-W. Shu, *Positivity preserving high order well balanced discontinuous Galerkin methods for the shallow water equations,* Advances inWater Resources, 33 (2010), 1476-1493.

[32] T. Xiong, J.-M. Qiu and Z. Xu, *High order maximum-principle-preserving discontinuous Galerkin method for convection-diffusion equations*, SIAM Journal on Scientific Computing, 37 (2015), A583-A608.

[33] Z. Xu, *Parametrized maximum principle preserving flux limiters for high order schemes solving hyperbolic conservation laws: One-dimensional scalar problem*, Mathematics of Computation, 83 (2014), 310-331.

[34] D. Yang *A splitting positive definite mixed element method for miscible displacement of compressible flow in porous media,* Numerical Methods for Partial Differential Equations, 17 (2001), 229-249.

[35] J. Yang and Y. Chen, *A priori error estimates of a combined mixed finite element and discontinuous Galerkin method for compressible miscible displacement with molecular diffusion and dispersion*, Journal of Computational Mathematics, 28 (2010), 1005-1022.

[36] J. Yang, *A posteriori error of a discontinuous Galerkin scheme for compressible miscible displacement problems with molecular diffusion and dispersion*, International Journal for Numerical Methods in Fluids, 65 (2011), 781-797.

[37] J. Yang and Y. Chen, *A priori error analysis of a discontinuous Galerkin approximation for a kind of compressible miscible displacement problems*, Science China Mathematics, 53 (2010), 2679-2696.

[38] Y. Yang and C.-W. Shu, *Discontinuous Galerkin method for hyperbolic equations involving δ-singularities: Negative-order norm error estimates and applications*, Numerische Mathematik, 124,(2013),753-781.

[39] Y. Yang, D. Wei and C.-W. Shu, *Discontinuous Galerkin method for Krause's consensus models and pressureless Euler equations,* Journal of Computational Physics, 252 (2013), 109-127.

[40] F. Yu, H. Guo, N. Chuenjarern and Y. Yang, *Conservative local discontinuous Galerkin method for compressible miscible displacements in porous media*, Journal of Scientific Computing, 73 (2017), 1249-1275.

[41] Y. Yuan, *The characteristic finite difference fractional steps methods for compressible two-phase displacement problem*, Science in China Series A-Mathematics, 42 (1999), 48-57.

[42] Y. Yuan, *The upwind finite difference fractional steps methods for two-phase compressible flow in porous media*, Numerical Methods Partial Differential Equations, 19 (2003), 67-88.

[43] Y. Yuan, *The modified upwind finite difference fractional steps method for compressible two-phase displacement problem*, Acta Mathematicae Applicatae Sinica, 20 (2004), 381-396.

[44] X. Zhang and C.-W. Shu, *On maximum-principle-satisfying high order schemes for scalar conservation laws*, Journal of Computational Physics, 229 (2010), 3091-3120.

[45] X. Zhang and C.-W. Shu, *On positivity preserving high order discontinuous Galerkin schemes for compressible Euler equations on rectangular meshes*, Journal of Computational Physics, 229 (2010), 8918-8934.

[46] X. Zhang and C.-W. Shu, *Positivity-preserving high order discontinuous Galerkin schemes for compressible Euler equations with source terms*, Journal of Computational Physics, 230 (2011), 1238-1248.

[47] X. Zhang, Y. Xia and C.-W. Shu, *Maximum-Principle-Satisfying and Positivity-Preserving High Order Discontinuous Galerkin Schemes for Conservation Laws on Triangular Meshes*, Journal of Scientific Computing, (2012), 50: 29-32.

[48] Y. Zhang, X. Zhang and C.-W. Shu, *Maximum-principle-satisfying second order discontinuous Galerkin schemes for convection-diffusion equations on triangular meshes*, Journal of Computational Physics, 234 (2013), 295-316.

[49] X. Zhao, Y. Yang and C. Seyler, *A positivity-preserving semi-implicit discontinuous Galerkin scheme for solving extended magnetohydrodynamics equations*, Journal of Computational Physics, 278 (2014), 400-415.